Available online at www.sciencedirect.com
SCIENCE DIRECT®
Remote Sensing of Environment 90 (2004) 210–220
Remote Sensing of Environment
www.elsevier.com/locate/rse

Bidirectional reflectance of Earth targets: Evaluation of analytical models using a large set of spaceborne measurements with emphasis on the Hot Spot

F. Maignan[a], F.-M. Bréon[a,*], R. Lacaze[b]

[a] *Laboratoire des Sciences du Climat et de l'Environnement, CEA/DSM/LSCE, 91191 Gif sur Yvette, France*
[b] *Medias-France, CNES, bpi 2102, 18, avenue Edouard Belin, 31401 Toulouse Cedex 9, France*

Received 19 August 2003; received in revised form 8 December 2003; accepted 13 December 2003

Abstract

Multidirectional observation from the spaceborne POLDER (Polarization and Directionality of the Earth Reflectance) instrument makes it possible to measure the bidirectional reflectance of a large variety of Earth targets. A careful selection of cloud-free measurements with a large directional coverage lead to about 22,000 sets of measured Bidirectional Reflectance Distribution Functions (BRDFs). This data set is used to evaluate the ability of analytical models to reproduce the observed directional signatures. Among those evaluated, the best models appear to be the three-parameter linear Ross–Li model, and the nonlinear Rahman–Pinty–Verstraete (RPV) model. On the other hand, all models fail to accurately reproduce the sharp reflectance increase (hot spot) close to the backscattering direction. Based on physical considerations, we suggest a modification of the Ross–Li model, without adding a free parameter, to account for the complex radiative transfer within the canopy that leads to the hot spot signature. The modified linear model performs better than all others, including the RPV nonlinear model. Although the correction modifies the retrieved directional signature parameters, it does not change significantly the surface albedo estimates.

Keywords: Reflectance; BRDF; Hot Spot; Model; POLDER

1. Introduction

The Bidirectional Reflectance Distribution Function (BRDF) quantifies the angular distribution of radiance reflected by an illuminated surface. A proper estimate of these functions is necessary for land surface studies to:

- correct bidirectional effects in time series of vegetation indices and reflectances (e.g. Leroy & Roujean, 1994; Wu et al., 1995);
- evaluate the coupling between surface reflectance and atmospheric scattering for proper atmospheric correction (Vermote et al., 1997);
- classify land surface cover (Hyman & Barnsley, 1997; Zhang et al., 2002);
- use the directional signature for the estimate of surface parameters such as leaf area index and other biophysical parameters (Knyazikhin et al., 1998; Bicheron & Leroy, 1999);
- estimate the albedo from reflectance measurements (Wanner et al., 1997; Cabot & Dedieu, 1997).

BRDFs have been measured in the field (e.g. Kimes, 1983; Deering et al., 1992) or from airborne instruments (Irons et al., 1991; Leroy & Bréon, 1996). Such measurements provide an adequate directional sampling, but with a rather poor sampling of the natural biome variability. Surface reflectance directional signatures have also been measured from space with the AVHRR (e.g. Gutman, 1987) or the ATSR (Godsalve, 1995). These instruments provide a large sampling of Earth targets, but the coverage is limited within the directional space due to the observation geometry of these sensors. The MISR instrument onboard the Terra platform provides an extended viewing geometry along the satellite track with a spatial resolution of 275 m in "Local Mode" and 1.1 km in "Global Mode" (Diner et al., 1998). The along-track viewing geometry provides a 1D sampling

* Corresponding author. Tel.: +33-169089455; fax: +33-169087716.
E-mail address: fmbreon@cea.fr (F.-M. Bréon).

0034-4257/$ - see front matter © 2004 Elsevier Inc. All rights reserved.
doi:10.1016/j.rse.2003.12.006

within the hemisphere, which may be complemented by MODIS measurements (cross-track sampling, Lucht & Lewis, 2000). Despite its lower spatial resolution (on the order of 6 km), the spaceborne POLDER (Polarization and Directionality of the Earth Reflectance) instrument (Deschamps et al., 1994) provides a much better directional sampling that is adequate to measure the BRDF up to about 65° of viewing angles.

Many models have been proposed to simulate or reproduce the directional signatures of land surface reflectance. These models may be classified into (i) ray-tracing simulations (e.g. Gascon et al., 2001; Gemmell & McDonald, 2000); (ii) complex models that fully analyze the radiative transfer within the canopy (e.g. Chen & Leblanc, 1997; Kuusk, 1995); (iii) analytical models based on various approximations of the radiative transfer (e.g. Roujean et al., 1992; Rahman et al., 1993), and (iv) empirical models (e.g. Walthall et al., 1985). The quality of these models can be evaluated either through the comparison of simulations by other models of higher complexity, or through a comparison with measurements.

In this paper, we evaluate a set of analytical models against spaceborne measurements from the POLDER instrument, in line with a former study by Bicheron and Leroy (2000) over a more limited data set. We only deal with analytical models (classes (iii) and (iv) above) because the others cannot be easily inverted on a set of measurements. The model quality is assessed from the root-mean square error (i.e. the measurement-model difference) after parameter inversion. The comparison indicates that the largest differences are generally observed close to backscattering, which suggests a physically based improvement of the existing models. In the last section, we discuss the impact of the hot spot on the albedo estimate.

2. Data

POLDER-1 (Polarization and Directionality of the Earth Reflectance) was launched onboard the ADEOS-1 platform in August 1996. Despite a premature failure of the platform solar panel that doomed all instruments onboard, 8 months of reflectance measurements have been acquired by POLDER. The major specificity of the radiometer that is exploited in this paper is the multidirectional capability. The bidimensional CCD matrix makes it possible to observe, at a given time, a bidimensional field of view. There is a large overlap of successive snapshots acquired every 20 s. As a consequence, a given Earth target is observed from up to 14 different directions as the satellite overflies the surface. In addition, during the following days, additional measurements of the same target are acquired from yet other directions. A monthly synthesis generates a very dense and complete coverage of the viewing geometry up to viewing angles of 65°. On the other hand, there is limited variation of the sun angle during this period. In this paper, we assume no temporal variation of the target during the period of synthesis. Clearly, this generates some intrinsic variance, in particular for snow-melting targets or for rapid vegetation growth. Another limitation of the measurements is the coarse spatial resolution ($\approx 6 \times 6$ km) that may lead to a significant fraction of mixed targets.

Cloud contaminated measurements are rejected using a series of tests (Bréon & Colzy, 1999). Data processing then performs the correction for atmospheric absorption (O_3, O_2 and H_2O) and molecular scattering (Leroy et al., 1997). It yields the so-called Level-2 products, on a per orbit basis, with up to 14 different measurements per channel for a given target. Temporal synthesis yields a much larger directional coverage, with a density that depends mostly on the cloud cover. Multi-temporal, multidirectional observations of the reflectance are available for all terrestrial 6-km pixels over the Earth. To constitute a diverse—yet manageable—data set of Earth directional signatures, a sample was performed among the monthly synthesis. The sampling is based on criteria of:

- directional coverage (many measurements available, well distributed over the hemisphere);
- variety of Earth targets (based on the 17 classes IGBP classification (Loveland et al., 2000), 8 months, 5 classes of latitude, and 12 classes of NDVI);
- quality of the measurements (based on the smoothness of the measurements on a multi-temporal basis).

The complete procedure (Lacaze, 2003) generated a set of 22,594 BRDFs that are used in the following.

3. BRDF models

In this paper, we evaluate three linear models in addition to a nonlinear one.

Linear models take the form:

$$R(\theta_s, \theta_v, \varphi) = k_0 + k_1 F_1(\theta_s, \theta_v, \varphi) + k_2 F_2(\theta_s, \theta_v, \varphi) + \ldots + k_n F_n(\theta_s, \theta_v, \varphi) \quad (1)$$

where θ_s, θ_v and φ are the solar zenith, view zenith and relative azimuth angles, respectively, F_i are a-priori kernels based on either physical or empirical considerations, and k_i are free parameters to be inverted on the measurements. In general, the linear models proposed in the literature have three parameters ($n=2$).

The modified Walthall model (Walthall et al., 1985; Nilson & Kuusk, 1989) is a four-parameter linear model based on empirical considerations.

$$F_1 = \theta_s^2 + \theta_v^2 \quad F_2 = \theta_s^2 \theta_v^2 \quad F_3 = \theta_s \theta_v \cos\varphi \quad (2)$$

The Roujean model (Roujean et al., 1992) is a three-parameter linear model. Kernels F_1 and F_2 have been derived from physical considerations of the radiative transfer at the surface. F_2 attempts an approximation of the radiative transfer within a vegetation canopy, whereas F_1 estimates the directional reflectance of a flat surface with randomly distributed and oriented protrusions. Note that, because kernel F_2 is based on Ross (1981) modeling and assumes a large optical thickness, it is often referred to as *Ross thick* (Wanner et al., 1995).

$$F_1 = \frac{1}{2\pi}[(\pi-\varphi)\cos\varphi + \sin\varphi]\tan\theta_s\tan\theta_v - \frac{1}{\pi}[\tan\theta_s + \tan\theta_v + \Delta(\theta_s,\theta_v,\varphi)]$$

$$F_2 = \frac{4}{3\pi}\frac{1}{\cos\theta_s+\cos\theta_v}\left[\left(\frac{\pi}{2}-\xi\right)\cos\xi + \sin\xi\right] - \frac{1}{3} \quad (3)$$

where ξ is the phase angle given by:

$$\cos\xi = \cos\theta_s\cos\theta_v + \sin\theta_s\sin\theta_v\cos\varphi \quad (4)$$

and Δ quantifies the horizontal distance between the sun and view directions:

$$\Delta(\theta_s,\theta_v,\varphi) = \sqrt{\tan^2\theta_s + \tan^2\theta_v - 2\tan\theta_s\tan\theta_v\cos\varphi} \quad (5)$$

This model has been used for a global quantification of directional effects (Lovell & Graetz, 2002; Leroy et al., 2003).

The "Ross Thick Li Sparse reciprocal combination", hereafter referred to as Ross–Li model, was selected for the processing of MODIS land surface measurements (Lucht et al., 2000). In the operational processing, it is a linear three-parameter model, as in Eq. (1). On the other hand, the F_1 kernel includes two additional parameters that may be freed, in which case the model becomes a five-parameter nonlinear model. The F_2 kernel is equivalent to the F_2 kernel of the Roujean model (Eq. (3)). The F_1 kernel accounts for the mutual shadowing of protrusions.

$$F_1 = \frac{m}{\pi}(t - \sin t\cos t - \pi) + \frac{1+\cos\xi}{2\cos\theta_s\cos\theta_v}$$

$$\cos t = \frac{2}{m}\sqrt{\Delta^2 + (\tan\theta_s\tan\theta_v\sin\varphi)^2}$$

$$m = \frac{1}{\cos\theta_s} + \frac{1}{\cos\theta_v} \quad (6)$$

The Rahman–Pinty–Verstraete (hereafter RPV) model (Rahman et al., 1993) is a three-parameter nonlinear semi-empirical model. It is based on the product of three functions: the first one, derived from Minnaert (1941), is a combination of the view and sun zenith angles; an Henyey–Greenstein function $P(\xi)$ accounts for the phase function of scattering elements; while $(1+R(\xi))$ explicitly accounts for the hot spot:

$$R(\theta_s,\theta_v,\varphi) = k_0\frac{\cos^{k_2-1}\theta_s\cos^{k_2-1}\theta_v}{(\cos\theta_s+\cos\theta_v)^{1-k_2}}P(\xi)1+R(\xi)]$$

$$P(\xi) = \frac{1-k_1^2}{\left(1+k_1^2-2k_1\cos(\pi-\xi)\right)^{3/2}}$$

$$R(\xi) = \frac{1-k_0}{1+\Delta(\theta_s,\theta_v,\varphi)} \quad (7)$$

Inversion of the parameters of such a nonlinear model is very time-consuming, impeding its use in an operational processing line of spatial measurements. In order to solve this problem, a linear version was derived (Engelsen et al., 1996):

$$\ln\left(\frac{R(\theta_s,\theta_v,\varphi)}{H}\right) = \ln k_0 - k_1\cos\xi + (k_2-1)\ln(\cos\theta_s\cos\theta_v \times (\cos\theta_s+\cos\theta_v))$$

$$H = 1 + \frac{1-\bar{R}}{1+\Delta(\theta_s,\theta_v,\varphi)} \quad (8)$$

where $\bar{R}$ is the mean reflectance over the hemisphere.

In the next section, we evaluate the capability of these analytical models to reproduce the directional signatures as observed by POLDER. The model parameters $[K]$ are inverted so as to minimize the Root Mean Square (hereafter RMS) difference between the measurements and the model values. For the linear models, this inversion is a simple matrix inversion:

$$[K] = ([F]^t[F])^{-1}[F]^t[R] \quad (9)$$

where $[R]$ is a $1\times N$ matrix, representing the column vector of the N measured reflectances and $[F]$ is an mxN matrix, representing for each of the m kernels the column vector of the kernel values for each of the N measurement geometries.

For the RPV nonlinear model, we use the Interactive Data Language (IDL, Research Systems) POWELL procedure, with a fractional tolerance of 10^{-6} and a maximum allowed number of iterations equal to 5000. The POWELL procedure is used here to minimize the mean-square error, using the Powell method (Press et al., 1993).

4. Results

Fig. 1 shows a typical example of a measurement-model comparison. The three rows of figures correspond to three channels at 565 nm (green), 670 nm (red) and 865 nm (near IR). The first column is a graphical representation of the

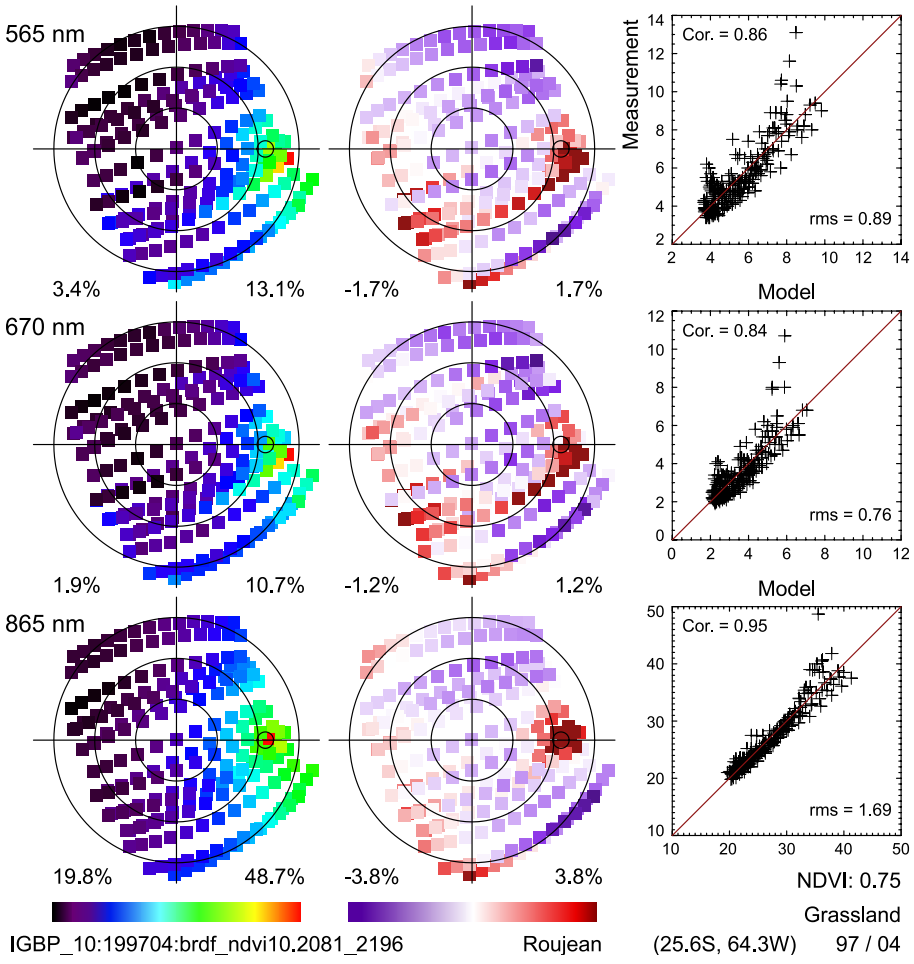

Fig. 1. Graphical representation of one BRDF sample of the database and comparison to the fitted Roujean model. Each line concerns a different POLDER channel: 565, 670 and 865 nm from top to bottom. On the leftmost column, reflectances are plotted on a polar diagram: constant viewing zenith angles are represented as circles every 20°; the principal plane is on the horizontal straight line with backscattering to the right. The small circle corresponds to the median sun angle during the period of synthesis and indicates the hot spot direction. The central column is measurement-model difference in reflectance. Note that the ranges for the color scales vary with the channel and are indicated on the bottom of each plot. The rightmost column is a scatter plot of measured and modeled reflectances. The data were acquired during April 1997 over northern Argentina.

color-coded measurements. The second column shows the difference between the measurements and the model, after parameter inversion. Finally, the third column is a scatter plot of the measured and modeled values.

Although Fig. 1 is only one measurement among the more than 22,000 cases of the database, and is based on the Roujean model for column two and three, it is rather typical for a vegetation cover. We now discuss, based on this figure, several findings that apply to the vast majority of analyzed cases.

In absolute values, the directional variability of the reflectance is larger in the near IR than in the visible part of the spectrum. On the other hand, in relative values, the directional signature is larger in the visible. On the example shown in Fig. 1, the reflectances in the green and red vary by a factor of more than 4, whereas the near infrared reflectance varies by a factor between 2 and 3. The largest reflectances are always observed close to the backscattering direction, except for (i) snow targets, easily identified by a large reflectance in all three bands, that show a broad maximum in the forward direction, and (ii) a few cases with a specular maximum indicative of the presence of water bodies in the pixel. Note that the measurement observed within one degree of the backscattering direction is much larger than those at 5° or more. The reflectance increase (≈ 0.05 in the visible, 0.15 in the near IR) has the same order of magnitude as the reflectance outside of the hot spot feature.

The model reproduces closely the measured signature. This is apparent both on the scatter plots (right column) but also based on the range of measurement-model difference (middle column) with respect to the range of measurements (left column).

The measurement-model difference is on the order or less than a few percent. It is slightly larger in the near IR, although, the relative error is much smaller in this channel. Clearly, both the measurements and the model errors contribute to the difference shown in the middle column of Fig. 1. The most obvious model error is the inability to reproduce

the large reflectance increase close to backscattering. Other deficiencies are apparent where positive or negative measurement-model differences are observed on a large directional portion of the BRDF. On the other hand, there are also some significant measurement errors. Some lines of measurements, corresponding to a single satellite pass, show a reflectance larger than their neighbours (easily seen in the measurement-model column). This may be interpreted by an undetected cloud or aerosol contamination. This interpretation implies that the error is larger in the visible that in the near IR. This is true in absolute (because the aerosol optical thickness decreases with an increase of wavelength) but mostly in relative since the surface signal is then much smaller.

The analysis of Fig. 1 and all other similar plots based on different surface targets clearly indicates that the signal to noise in the measured directional signatures is much better in the near IR than in the visible. This is easily explained as the directional effect amplitude (the signal) scales roughly with the surface reflectance, which is generally larger in the near IR. In addition, the "noise" is mostly generated by atmospheric scattering (undetected clouds, aerosols, molecules), which tends to be larger in the visible. Both effects contribute to a measurement of better quality in the near IR. For this reason, the following analysis is based on the 865-nm measurements. In the discussion section, we comment the generalization to visible channels.

We now compare the measurement-model RMS error (hereafter RMSE) when using different models. The RMSE contains contributions from the measurement errors and the model errors. It is expected that, when comparing two models, the measurement contribution to the RMSE is very similar for the two. Thus, in general, a lower RMSE indicates that the model performs better in fitting the surface BRDF. There may be exceptions to this rule when a measurement error is better fitted by a model that performs poorly at reproducing the real surface BRDF. However, such cases cannot hide a general trend.

Among the models that are evaluated here, the modified Walthall model is clearly the least performing (Fig. 2a) despite a larger degree of freedom (four parameters) which indicates the advantage of a physical—even approximated—a priori modeling of the surface radiative transfer as used in the other models. Among the three other linear models, the Ross–Li one is doing better than the Engelsen one (Fig. 2c), which is itself better than the Roujean one

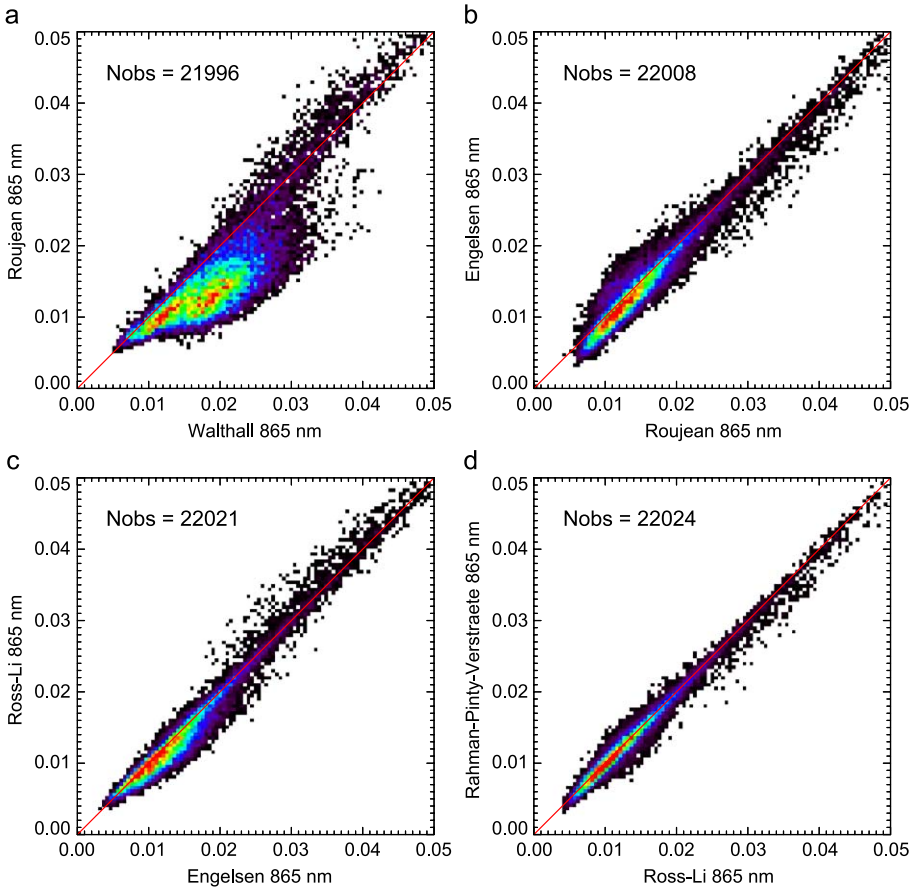

Fig. 2. Comparison of the performances of five major BRDF analytical models. Each plot is a bidirectional histogram of the RMSEs at 865 nm for two different models. RMSEs are calculated for each pixel in the BRDF database. Only pixels whose RMSE is lower than 0.05 for both models are shown, which includes more than 97% of the database; the resulting number of observations (Nobs) is indicated on the upper-left corner of each figure.

(Fig. 2b). The Ross–Li linear model and the RPV get quite comparable results (Fig. 2d). These conclusions are consistent with Bicheron and Leroy (2000), which were obtained with a reduced 400 BRDF database.

Fig. 2 shows that, for large RMSE values, i.e. targets that are poorly fitted by the models, the nonlinear RPV model and its linear version perform significantly better than the Ross–Li one. These high values (above 0.3) are related to snow measurements, in which case the Ross–Li model hypotheses are not adapted. In fact, none of the models analyzed here are designed for snow targets and they all performed poorly in such case. Nevertheless, the RPV model and its linear version, which have a stronger empirical formulation and are more flexible, are better adapted and tend to perform better than the others.

5. Improvement of the *Ross thick* kernel and validation

The F_2 kernel in Eq. (3) was originally proposed by Roujean et al. (1992) based on radiative transfer within a turbid vegetation canopy. Wanner et al. (1995) renamed this kernel as *Ross thick*, because it applies to a thick canopy. The same kernel is used in the Ross–Li linear model that was shown above to be the most successful, together with RPV, at reproducing the observed BRDFs. On the other hand, although this kernel aims at modeling the radiative transfer within the vegetation canopy, it does not account for the so-called hot spot or opposition effect, which occurs when viewing and illumination directions coincide. For viewing geometries close to backscattering, a strong reflectance peak is observed that is not accounted for in the linear model, as shown in Fig. 1. Several studies address the objective of improving the model capabilities to reproduce the hot spot feature, mainly through the addition of a specific kernel (see for example Chen & Cihlar, 1997). Below, we propose to rather modify the kernel, based on physical considerations.

In Roujean et al. (1992) the reflectance of a theoretical vegetation canopy is considered based on the following hypotheses:

- the scattering medium is composed of small-scale elements (leaves);
- these elements are randomly distributed within the canopy;
- they are randomly oriented (spherical distribution);
- only single scattering is considered (multiple scattering is assumed isotropic and is therefore accounted for in another kernel);
- the medium is optically thick.

With these hypotheses, the canopy reflectance is shown to be:

$$R = \frac{2\,\rho_{leaf}}{3(\cos\theta_s + \cos\theta_v)} \frac{(\pi - 2\xi)\cos\xi + 2\sin\xi}{\pi} \qquad (10)$$

In this equation, the second fraction corresponds to the scattering phase function of the leaves (Ross, 1981) whereas the first one results from transmission effects within the canopy.

These are the exact same hypotheses as in Bréon et al. (2002) that specifically addresses the hot spot modeling. The model in this paper computes the correlation in transmission (gap fraction) between the incoming and outgoing directions. It shows that accounting for the correlation in the transmission increases the single scattering reflectance by a factor $1+(1+\xi/\xi_0)^{-1}$ where ξ_0 is a characteristic angle that can be related to the ratio of scattering element size and the canopy vertical density. At backscattering, the predicted reflectance is twice as much as when correlated transmission is not accounted for. For large phase angles, the ratio is close to 1. The hot spot modeling has been validated against measurements acquired with the spaceborne POLDER instrument with a very high directional resolution, i.e. on the order of 0.3° (Bréon et al., 2002; Camacho de Coca et al., 2004). In particular, it was shown that the shape of the hot spot (i.e. the reflectance decrease with an increase of ξ) is very well reproduced by the function (see an example in Fig. 3.

Therefore, it appears possible to merge the two models into:

$$R = \frac{2\rho_{\text{leaf}}}{3\,(\cos\theta_s + \cos\theta_v)} \frac{(\pi - 2\xi)\cos\xi + 2\sin\xi}{\pi} \times \left(1 + \frac{1}{1+\xi/\xi_0}\right) \qquad (11)$$

In addition, the Bréon et al. model fit to the spaceborne measurements over a wide variety of surface covers indi-

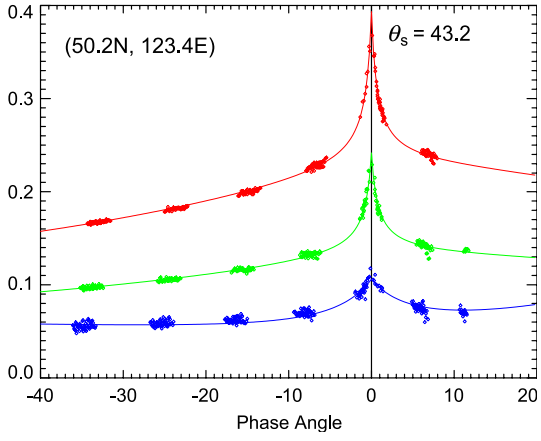

Fig. 3. Hot spot directional signature as observed from the POLDER spaceborne instrument over a 7 × 7 pixels area. The measured reflectance is shown as a function of phase angle ξ. A minus sign has been applied to the phase angle when $\theta_v\cos\varphi < \theta_s$. The wavelength is 565, 670 and 865 nm from bottom to top. The line shows the result of a best fit through the data points using the nonlinear function $R_m = k_0 + k_1F_1(\theta_s,\theta_v,\varphi) + k_2F_2(\theta_s,\theta_v,\varphi)(1+A)/(1+\xi/\xi_0)$ where F_1 and F_2 are given in Eqs. (3) and (6) and k_0, k_1, k_2, A and ξ_0 are free parameters. The data were acquired on April 12th, 1997 over the Northern part of China (Khingan Range).

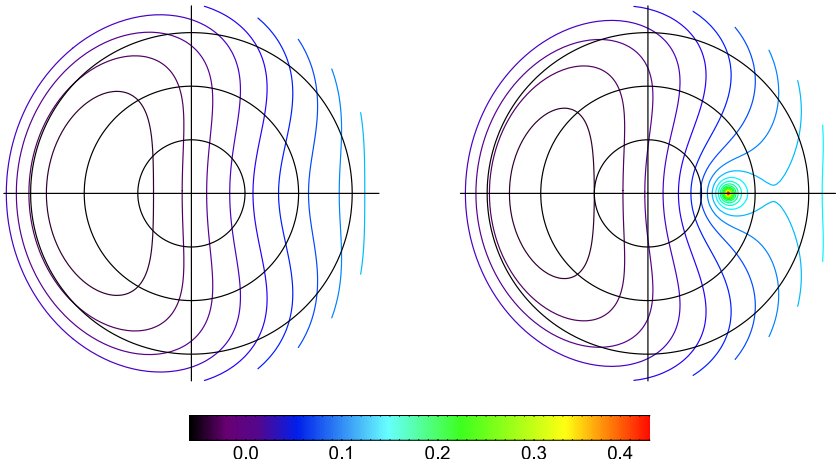

Fig. 4. Isocontours of the *Ross thick* kernel with its original version of Eq. (3) (left figure) and the new version of Eq. (12) (right figure) that includes the hot spot modeling.

cates a small variation of ξ_0, most of the targets being in the range 1–2°. Thus, to avoid the addition of a free parameter in the BRDF modeling, we suggest taking a constant value of $\xi_0 = 1.5°$. This simple modeling of a thick vegetation canopy leads to a modified version of the F_2 kernel of Eq. (3) to:

$$F_2^{HS}(\theta_s, \theta_v, \varphi) = \frac{4}{3\pi} \frac{1}{\cos\theta_s + \cos\theta_v} \left[\left(\frac{\pi}{2} - \xi \right) \cos\xi + \sin\xi \right] \times \left(1 + \left(1 + \frac{\xi}{\xi_0} \right)^{-1} \right) - \frac{1}{3} \quad (12)$$

Note that we leave the constant at its original value ($-1/3$) to minimize the change in the kernel and the expected retrieved parameters (the factor in parentheses is close to 1 for most directions, i.e. for phase angles larger than a few degrees). On the other hand, with this particular choice, the kernel does not fulfil the original requirement of $F_2^{HS}(0,0,\varphi) = 0$, necessary to interpret k_0 as the reflectance for both the sun and the observer at zenith. However, we believe that the original model, which did not account for the hot spot effect, probably fails when the illumination and view directions coincide, since such geometric configuration is favorable to a hot spot contribution. The F_2 kernel and its modified version F_2^{HS} are shown in Fig. 4.

The improvement brought to the Roujean and Ross–Li models by adding the hot spot modeling to the *Ross thick* kernel may be quantified as above, through a statistical evaluation of the RMSE to the observed reflectances. The comparisons of these RMSEs with the original and corrected versions are shown in Fig. 5. There is a clear improvement of the measurement-model comparison for most of the targets. For the targets that have a RMSE less than 0.02, the RMSE relative decrease is on the order of 10%.

With the hot spot modeling introduced in the kernel, the linear Ross–Li model now performs better than the nonlinear RPV model (Fig. 6a). In addition, the linear model superiority is mostly apparent for vegetated targets identi-

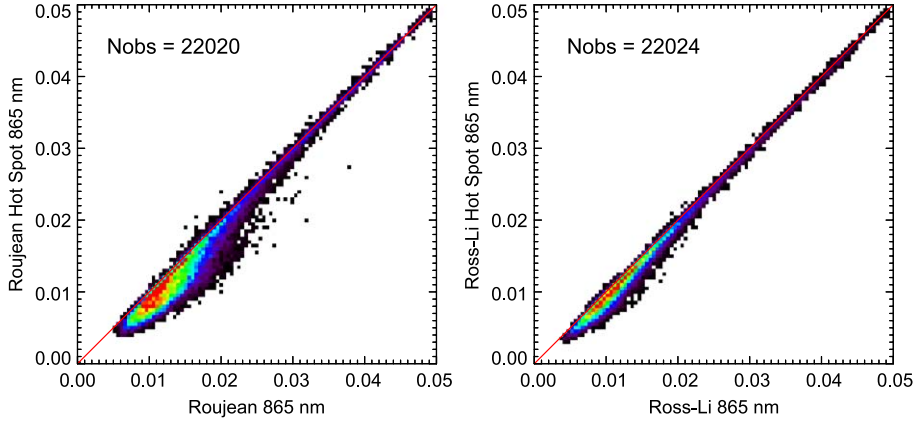

Fig. 5. Comparison of the performances of the Roujean (left) and Ross–Li (right) models, when using the original F_2 function (Eq. (3)) and that with the hot spot modeling (Eq. (12)). Each plot is a bidirectional histogram of the RMSEs at 865 nm for the two different models. RMSEs are calculated for each pixel in the BRDF database. Only pixels whose RMSE is lower than 0.05 for both models are shown.

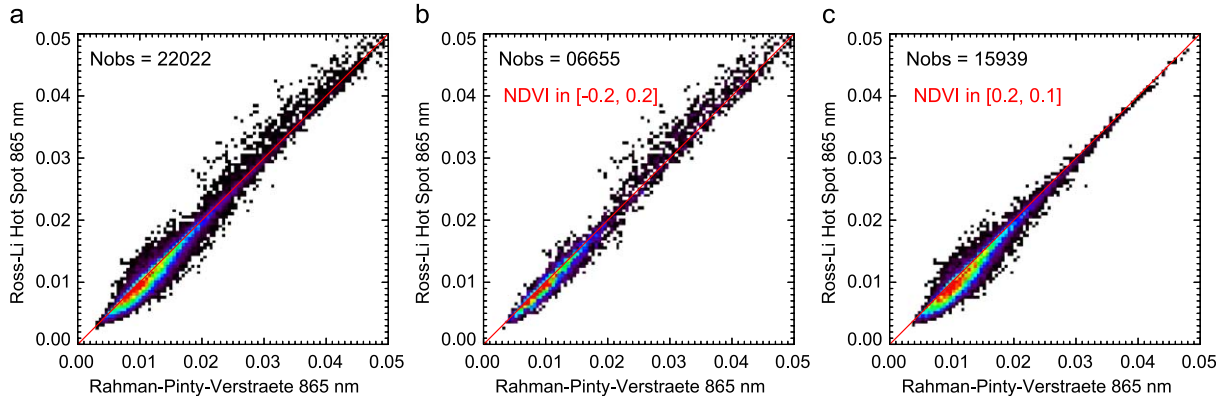

Fig. 6. Same as Fig. 5 but for the Ross–Li Hot Spot and the RPV models. (a) is for all targets of the database. The other figures are for low (b) and medium–high (c) values of NDVI.

fied by a NDVI greater than 0.2 (Fig. 6c). For lower values of the NDVI, the two model performances are equivalent (Fig. 6b). The larger improvement for large NDVIs is expected since the hot spot is a directional signature generated by radiative transfer and scattering within a volume, such as a vegetation canopy, and not by reflectance over a rough surface.

6. Discussion

With the addition of the two hot spot corrected models, we now have seven analytical models to evaluate. Fig. 7 shows the cumulative histograms of the RMSEs computed over the full data set and for all three spectral bands (green, red and near IR). Table 1 gives the median values of the RMS errors both in the visible and near IR. Both the figure and table demonstrate that the corrected Ross–Li model, including the hot spot function, performs better than any other model. Note that the relative improvement of the RMSEs is very significant for the low values of the cumulative histogram, which correspond to the best quality measurements. The advantage brought by a better model is mostly apparent when inverted against high signal to noise measurements. On the other hand, for the low quality targets (high values of the cumulative histograms), the nonlinear RPV model performs slightly better. Note also that the Roujean model, with the Hot Spot modeling correction, performs better than the original Ross–Li or the RPV models. However, there is apparently no argument to use the corrected Roujean model rather than the corrected Ross–Li one.

Roughly 10% of the targets in the database show an RMSE larger than 0.03 whichever model is used. A large fraction of those correspond to snow targets, for which none of the tested analytical models is well suited. Other targets show a very strong reflectance in the glint direction, which indicates the presence of water bodies in the pixel. A single directional observation with a measured reflectance much larger than the model can generate a large RMSE. Finally, some targets show rather noisy measurements with cloud contamination or varying snow coverage. For noise-free measurements, the models, and in particular the hot spot modified Ross–Li one provide astonishing accurate fits of the measurements, with correlation of up to 0.98 and RMSEs of less than 6.10^{-3} when the measurements variability is larger than 0.2.

The results in this paper were mostly based on 865-nm measurements because this band shows directional signatures with the highest signal to noise. Fig. 7 and Table 1 demonstrate that the same ranking of models is found in all three bands. The RMSE are slightly lower in the visible bands than in the near IR, but these are for much smaller amplitudes of the directional effects. The model-measurement correlation is much less in the visible than in the near IR. A question of importance is whether this lower correlation indicates that the BRDF models perform poorly, or if it is only a consequence of the measurement lower quality. As said above, the noise in the measurements, due to aerosol, cloud or snow contamination is similar or larger in the visible than in the near IR. Because the signal (i.e. the reflectance directional variations) is much smaller in the visible, the measurement signal to noise is lower. On the other hand, the theoretical development of all models is based on the single reflectance approximation. This approximation is more valid in the visible than in the near IR. Thus, although there is no demonstration of that from the measurements, it is reasonable to assume that the models perform better, both in absolute and relative, in the visible than in the near IR.

We now evaluate the importance of hot spot modeling on the target albedo estimate. The hot spot generates a large reflectance increase, but limited to a small angular domain. As a consequence, the impact on the albedo is the product of a large and a small number. Based on the evaluation of the hot spot function and the typical hot spot widths, Bréon et al. (2002) predicts a negligible impact on the albedo. In addition, some of the measurements are affected by the hot

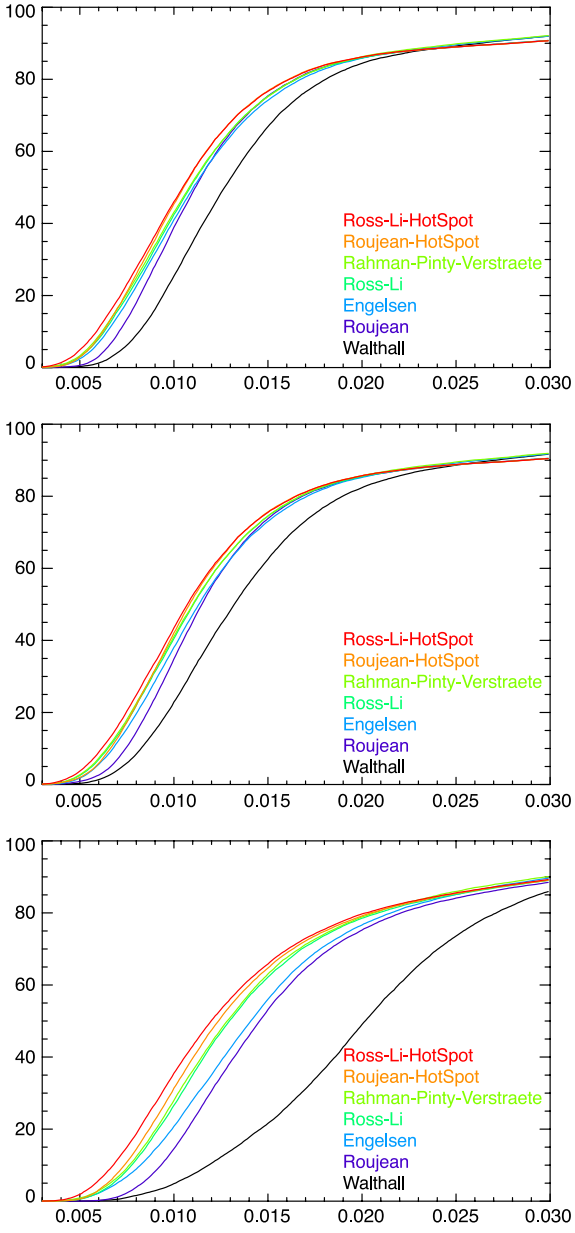

Fig. 7. Cumulative histograms of the RMSEs derived from the full BRDF data set when using all models that are discussed in this paper. POLDER channels 565, 670 and 865 nm are shown from top to bottom.

spot so that the model parameters somehow account for this reflectance increase: a model that does not account for the hot spot, fitted over well distributed measurements, tends to underestimate the BRDF close to backscattering and to overestimate it in other directions. This leads to a compensation of errors on the albedo estimate.

To compute the spectral albedo from the retrieved parameters, we have integrated the kernels over the full hemisphere:

$$G_i(\theta_s) = \frac{1}{\pi}\int_{\Omega} F_i(\theta_s, \theta_v, \varphi)\cos\theta_v d\omega \qquad (13)$$

Table 1

Fitted model	Median value			First decile		
	565 nm	670 nm	865 nm	565 nm	670 nm	865 nm
Walthall	1.280	1.330	2.030	0.811	0.820	1.179
Roujean	1.120	1.160	1.460	0.703	0.738	0.927
Engelsen	1.110	1.140	1.420	0.640	0.671	0.817
Ross–Li	1.100	1.110	1.300	0.625	0.644	0.770
RPV	1.090	1.110	1.290	0.613	0.638	0.757
Roujean Hot Spot	1.060	1.090	1.250	0.618	0.657	0.732
Ross–Li Hot Spot	1.060	1.080	1.210	0.584	0.611	0.672

RMSE (in reflectance × 100) median values and first decile for each model and all three bands: green (565 nm), red (670 nm) and near IR (865 nm). With the first decile, 10% of the targets have a lower RMSE (50% for the median).

Because some kernels tend to diverge at large zenith angles, we have limited their values to those obtained for an angle of 75°. The spectral albedos are then evaluated from the retrieved parameters through:

$$A(\theta_s) = k_0 + k_1 G_1(\theta_s) + k_2 G_2(\theta_s) \qquad (14)$$

where we take the solar zenith angle as the mean value over the measurements. This procedure is done independently on the Ross–Li inverted parameters and the same using the corrected F_2 kernel (with a different G_2). Fig. 8 shows the difference in the spectral albedo estimates. There is no significant bias in the retrieved albedos with the two methods. The RMS difference is on the order of 10^{-3}, which is less than 1% in relative units. For the visible channels, similar results are expected. Because the hot spot amplitude is smaller than at 865 nm (Bréon et al., 2002) the absolute impact on the albedo is necessarily smaller than 10^{-3}. On the other hand, because the reflectance relative increase due to the hot spot is larger in the visible, the corresponding impact on the albedo may be larger, up to 2% in relative.

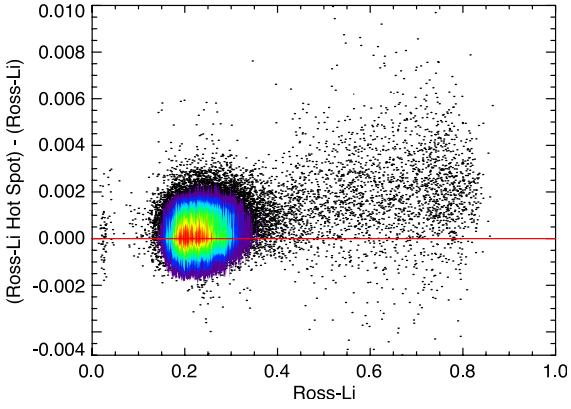

Fig. 8. Comparison of the estimated albedo (i.e. the reflectance integrated over the full hemisphere) when the measurements are fitted by the Ross–Li and the Ross–Li Hot Spot models. The figure shows a 2D histogram of the estimate difference as a function of one estimate.

7. Summary and conclusion

A large data set of spaceborne directional reflectance measurements allows an evaluation of various analytical models. A good fit of the measurements by a model is limited both by the noise on the measurements and the model quality. For the evaluation, near-infrared measurements are preferred to visible ones both because of the larger amplitude of the directional effects and because of the lower atmospheric perturbation. In term of RMS error, the relative difference between the models is rather small; i.e. the noise on the measurement has a larger impact than the model quality. Nevertheless, some models perform better than others at fitting the observed directional signature. The best fit is obtained with a linear three-parameter model, based on the so-called Ross–Li model, but with an explicit representation of the hot spot that accounts for the reflectance increase a few degrees around the backscattering direction. Typical RMS errors are on the order of 0.01 both in the visible and the near infra-red channels when the amplitude of the directional effects is on the order of a few percent in the visible, and 0.2 in the near-infrared.

The data set used in this paper is available to the scientific community together with analysis tools (Lacaze, 2003). It is well suited to evaluate reflectance models and to provide typical reflectance signatures for a wide variety of surface covers. Its main limitation is the low spatial resolution that implies a majority of mixed surface coverage.

Acknowledgements

The data in this paper were based on measurements acquired by the CNES/POLDER-1 instrument onboard the NASDA/ADEOS-1 platform. This database has been generated by Medias France from POLDER-1 level 2 products using original algorithms developed by Noveltis.

References

Bicheron, P., & Leroy, M. (1999). A method of biophysical parameter retrieval at global scale by inversion of a vegetation reflectance model. *Remote Sensing of Environment*, *67*, 251–266.

Bicheron, P., & Leroy, M. (2000). Bidirectional reflectance distribution function signatures of major biomes observed from space. *Journal of Geophysical Research*, *105*(21), 26669–26681.

Bréon, F. M., & Colzy, S. (1999). Cloud detection from the spaceborne POLDER instrument and validation against surface synoptic observations. *Journal of Applied Meteorology*, *38*, 777–785.

Bréon, F. M., Maignan, F., Leroy, M., & Grant, I. (2002). Analysis of hot spot directional signatures measured from space. *Journal of Geophysical Research*, *107*(16), 4282–4296.

Cabot, F., & Dedieu, G. (1997). Surface albedo from space: Coupling bidirectional models and remotely sensed measurements. *Journal of Geophysical Research*, *102*, 19645–19664.

Camacho-de Coca, F., Bréon, F.-M., Leroy, M., & Garcia-Haro, F. J. (2004). Airborne measurement of hot spot reflectance signatures. *Remote Sensing of Environment* (in press).

Chen, J. M., & Cihlar, J. (1997). A hot spot function in a simple bidirectional reflectance model for satellite application. *Journal of Geophysical Research*, *102*(25), 25907–25913.

Chen, J. M., & Leblanc, S. G. (1997). A four-scale bidirectional reflectance model based on canopy architecture. *IEEE Transactions on Geoscience and Remote Sensing*, *35*, 1316–1337.

Deering, D. W., Eck, T. F., & Grier, T. (1992). Shinnery oak bidirectional reflectance properties and canopy model inversion. *IEEE Transactions on Geoscience and Remote Sensing*, *30*, 339–348.

Deschamps, P. Y., Bréon, F. M., Leroy, M., Podaire, A., Bricaud, A., Buriez, J. C., & Sèze, G. (1994). The POLDER mission: Instrument characteristics and scientific objectives. *IEEE Transactions on Geoscience and Remote Sensing*, *32*, 598–615.

Diner, D. J., Beckert, J. C., Reilly, T. H., Bruegge, C. J., Conel, J. E., Kahn, R., Martonchik, J. V., Ackerman, T. P., Davies, R., Gerstl, S. A. W., Gordon, H. R., Muller, J. P., Myneni, R. B., Sellers, P. J., Pinty, B., & Verstraete, M. M. (1998). Multiangle Imaging SpectroRadiometer (MISR) description and experiment overview. *IEEE Transactions on Geoscience and Remote Sensing*, *36*(4), 1072–1087.

Engelsen, O., Pinty, B., Verstraete, M. M., & Martonchik, J. M. (1996). Parametric Bidirectional Reflectance Factor Models: Evaluation, Improvements and Applications. *EC Joint Research Center, Technical Report No. EUR 16426 EN,* 114 pp.

Gascon, F., Gastellu-Etchegorry, J. P., & Lefèvre, M. J. (2001). Radiative transfer model for simulating high-resolution satellite images. *IEEE Transactions on Geoscience and Remote Sensing*, *39*, 1922–1926.

Gemmell, F., & McDonald, A. J. (2000). View zenith angle effects on information content of three spectral indices. *Remote Sensing of Environment*, *72*(2), 139–158.

Godsalve, C. (1995). Bidirectional reflectance sampling by ATSR-2: A combined orbit and scan model. *International Journal of Remote Sensing*, *16*, 269–300.

Gutman, G. G. (1987). The derivation of vegetation indices from AVHRR data. *International Journal of Remote Sensing*, *8*, 1235–1243.

Hyman, A. H., & Barnsley, M. J. (1997). On the potential for land cover mapping from multiple view angle (MVA) remotely sensed information. *International Journal of Remote Sensing*, *18*, 2471–2475.

Irons, J. R., Ranson, K. J., Williams, D. L., Irish, R. R., & Huegel, F. G. (1991). An off-nadir pointing imaging spectroradiometer for terrestrial ecosystem studies. *IEEE Transaction in Geoscience and Remote Sensing*, *29*, 66–74.

Kimes, D. S. (1983). Dynamics of directional reflectance factor distributions for vegetation canopies. *Applied Optics*, *22*, 1364–1373.

Knyazikhin, Y., Martonchik, J. V., Diner, D. J., Myneni, R. B., Verstraete, M. M., Pinty, B., & Gobron, N. (1998). Estimation of vegetation canopy leaf area index and fraction of absorbed photosynthetically active radiation from atmosphere-corrected MISR data. *Journal of Geophysical Research*, *103*, 32239–32256.

Kuusk, A. (1995). A fast, invertible, canopy reflectance model. *Remote Sensing of Environment*, *51*, 342–350.

Lacaze, R. (2003). POLDER BRDF database — User Document, Edition 1—Revision 2. Available from http://medias.obs-mip.fr/postel/Projets/POLDER/produits/polder1/brdf.en.php.

Leroy, M., & Bréon, F. M. (1996). Surface reflectance angular signatures from airborne POLDER data. *Remote Sensing of Environment*, *57*, 97–107.

Leroy, M., Deuzé, J. L., Bréon, F. M., Hautecoeur, O., Herman, M., Buriez, J. C., Tanré, D., Bouffiès, S., Chazette, P., & Roujean, J. L. (1997). Retrieval of atmospheric properties and surface bidirectional reflectances over land from POLDER/ADEOS. *Journal of Geophysical Research*, *102*, 17023–17037.

Leroy, M., & Roujean, J. L. (1994). Sun and view angle corrections on reflectances derived from NOAA/AVHRR data. *IEEE Transactions on Geoscience and Remote Sensing*, *32*, 684–697.

Leroy, et al. (2003): POLDER Land Surfaces Level 3 advanced algorithms, http://smsc.cnes.fr/POLDER/SCIEPROD/lsp2algol3.htm.

Lovell, J. L., & Graetz, R. D. (2002). Analysis of POLDER-ADEOS data for the Australian continent: the relationship between BRDF and vegetation structure. *International Journal of Remote Sensing*, *23*(14), 2767–2796.

Loveland, T. R., Reed, B. C., Brown, J. F., Ohlen, D. O., Zhu, Z., Yang, L., & Merchant, J. W. (2000). Development of a global land cover characteristics database and IGBP DISCover from 1 km AVHRR data. *International Journal of Remote Sensing*, *21*(6–7), 1303–1330.

Lucht, W., & Lewis, P. (2000). Theoretical noise sensitivity of BRDF and albedo retrieval from the EOS-MODIS and MISR sensors with respect to angular sampling. *International Journal of Remote Sensing*, *21*(1), 81–98.

Lucht, W., Schaaf, C. B., & Strahler, A. H. (2000). An algorithm for the retrieval of albedo from space using semiempirical BRDF models. *IEEE Transactions on Geoscience and Remote Sensing*, *38*, 977–998.

Minnaert, M. (1941). The reciprocity principle in lunar photometry. *Astrophysical Journal*, *93*, 403–410.

Nilson, T., & Kuusk, A. (1989). A reflectance model for the homogeneous plant canopy and its inversion. *Remote Sensing of Environment*, *27*, 157–167.

Press, W. H., Flannery, B. P., Teukolsky, S. A., & Vetterling, W. T. (1993, January). *Numerical recipes in C: The art of scientific computing*. (2nd edition). Cambridge, UK: Cambridge University Press, 994 pp., ISBN: 0521431085.

Rahman, H., Pinty, B., & Verstraete, M. M. (1993). Coupled Surface-Atmosphere Reflectance (CSAR) Model 2. Semiempirical surface model usable with NOAA advanced very high resolution radiometer data. *Journal of Geophysical Research*, *98*(11), 20791–20801.

Ross, J. (1981). *The radiation regime and architecture of plant stands*. The Hague, Netherlands: Dr. W. Junk Publishers.

Roujean, J. L., Leroy, M., & Deschamps, P. Y. (1992). A bidirectional reflectance model of the earth's surface for the correction of the remote sensing data. *Journal of Geophysical Research*, *97*(18), 20455–20468.

Vermote, E. F., El Saleous, N. Z., Justice, C. O., Kaufman, Y. J., Privette, J., Remer, L., Roger, J. C., & Tanré, D. (1997). Atmospheric correction of visible to middle infrared EOS-MODIS data over land surface, background, operational algorithm and validation. *Journal of Geophysical Research*, *102*(14), 17131–17141.

Walthall, C. L., Norman, J. M., Welles, J. M., Campbell, G., & Blad, B. L. (1985). Simple equation to approximate the bidirectional reflectance from vegetative canopies and bare soil surfaces. *Applied Optics*, *24*(3), 383–387.

Wanner, W., Li, X., & Strahler, A. H. (1995). On the derivation of kernels for kernel-driven models of bidirectional reflectance. *Journal of Geophysical Research*, *100*(10), 21077–21089.

Wanner, W., Strahler, A. H., Hu, B., Lewis, P., Muller, J. P., Li, X., Schaaf, C. L. B., & Barnsley, M. J. (1997). Global retrieval of bidirectional reflectance and albedo over land from EOS MODIS and MISR data: Theory and algorithm. *Journal of Geophysical Research*, *102*(14), 17143–17161.

Wu, A., Li, Z., & Cihlar, J. (1995). Effects of land cover type and greenness on advanced very high radiometer bidirectional reflectances: Analysis and removal. *Journal of Geophysical Research*, *100*, 9179–9192.

Zhang, Y., Tian, Y., Myneni, R. B., Knyazikhin, Y., & Woodcock, C. E. (2002). Assessing the information content of multiangle satellite data for mapping biomes. I. Statistical analysis. *Remote Sensing of Environment*, *80*(3), 418–434.